

Nanoparticle Based Curve Arrays for Multirecognition Flexible Electronics

Meng Su, Fengyu Li,* Shuoran Chen, Zhandong Huang, Meng Qin, Wenbo Li, Xingye Zhang, and Yanlin Song*

Flexible electronics is blooming due to the increasing need of ultraintegrated circuits,^[1] wearable devices, and attached or embeddable electronics.^[2–5] Types of materials were developed and adopted for flexible circuit, capacitance, solar cell, display, and sensor. The polymer and organic materials present insufficient conductivity despite their advantages in flexibility and modifiability. Currently, to generate the flexibility, ultrathin films or straight lines on flexible substrate architectures have been employed.^[6,7] However, the rigid structures cannot offer extra stretchability with respect to the material's properties and tunable adaptability,^[8] which results in limitation on the bending or stretching extent. Thus, it is desirable to explore a feasible method for guiding conducting or semiconducting nanomaterials into elastomeric matrices (e.g., curves with various tortuosity morphologies). Here, we developed a facile fabrication process for nanoparticle-based curves through pillar-patterned silicon template-induced printing, and integrated the curves array as flexible sensors to perform complex recognition of human facial expression. The curves with different amplitudes and period lengths offer a stable stretching reversibility and arbitrary sensitivity adjustability. With sensitive skin moving perception, the printable nanocurve sensors run complicated facial expression recognition, and could be applied to skin micromotion manipulation auxiliary apparatuses for paraplegics or amputees.

Nanoparticle (NP) assemblies^[9–12] are verified as an efficient surface functional technology with photonic, electronic, and magnetic properties. Through manipulating the three-phase contact line (TCL), the nanoparticles contained in a liquid droplet will assemble and deposit following the TCL pattern. In our previous research, we developed the sandwich-shaped assembly system^[13] and inkjet-printing patterned substrates,^[14]

inducing nanoparticles to assemble into straight lines. The TCL manipulation with continuous singularity changing will benefit complicated pattern fabrication and printing of flexible devices. In this work, we explored a feasible method of pillar-patterned template-guided nanoparticle self-assembly into curves. NP curves with various ratios (termed as R) of the amplitude to the period length can be printed on a flexible film (e.g., poly(dimethylsiloxane) (PDMS)) by using the corresponding pillar-patterned silicon template. The resistive response of NP curves with different R to the strain is obviously differentiated. Combining the benefits of arbitrary adjustable curved design and differentiated resistance responses, the curve arrays provide a promising approach for flexible sensors. Accordingly, NP curve arrays with proper R on the flexible PDMS substrate were used as wearable sensors for small strains on human skin. Typically, smart facial expression recognition can be achieved by sensing the basic muscles essential for universal facial expression.^[15–17]

Figure 1 illustrates the fabrication process of the nanocurve-based strain sensor. Silver nanoparticles were guided into an array of curves on the flexible substrate through pillar-patterned template induced printing. These curves were patterned with various interdigitated golden electrodes by vacuum deposition. As-fabricated sensors were flexible and sensitive due to the optimized conductive curves arrays. The photo illustration

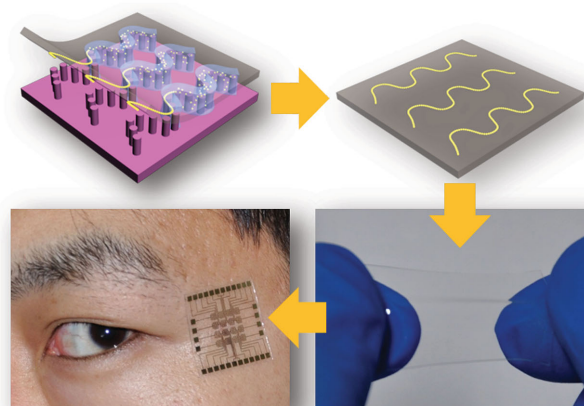


Figure 1. The schematic illustration of the NP curve array printed to flexible electronic devices and adopted to multianalysis for skin micromotion sensing. NP curve arrays were printed on the PDMS substrate by pillar-patterned template induced printing with silver nanoparticle ink. These flexible electronic sensors can be directly attached to human facial skin, and perform real-time multianalysis for skin micromotion monitoring.

Dr. M. Su, Prof. F. Li, Dr. S. Chen, Dr. Z. Huang, Dr. M. Qin, Dr. W. Li, Prof. X. Zhang, Prof. Y. Song
Key Laboratory of Green Printing
Institute of Chemistry
Chinese Academy of Sciences (ICCAS)
Beijing Engineering Research Center
of Nanomaterials for Green Printing Technology
Beijing National Laboratory for
Molecular Sciences (BNLMS)
Beijing 100190, P. R. China
E-mail: forrest@iccas.ac.cn; ylsong@iccas.ac.cn



Dr. M. Su, Dr. S. Chen, Dr. Z. Huang, Dr. M. Qin, Dr. W. Li
University of Chinese Academy of Sciences
Beijing 100049, P. R. China

DOI: 10.1002/adma.201504759

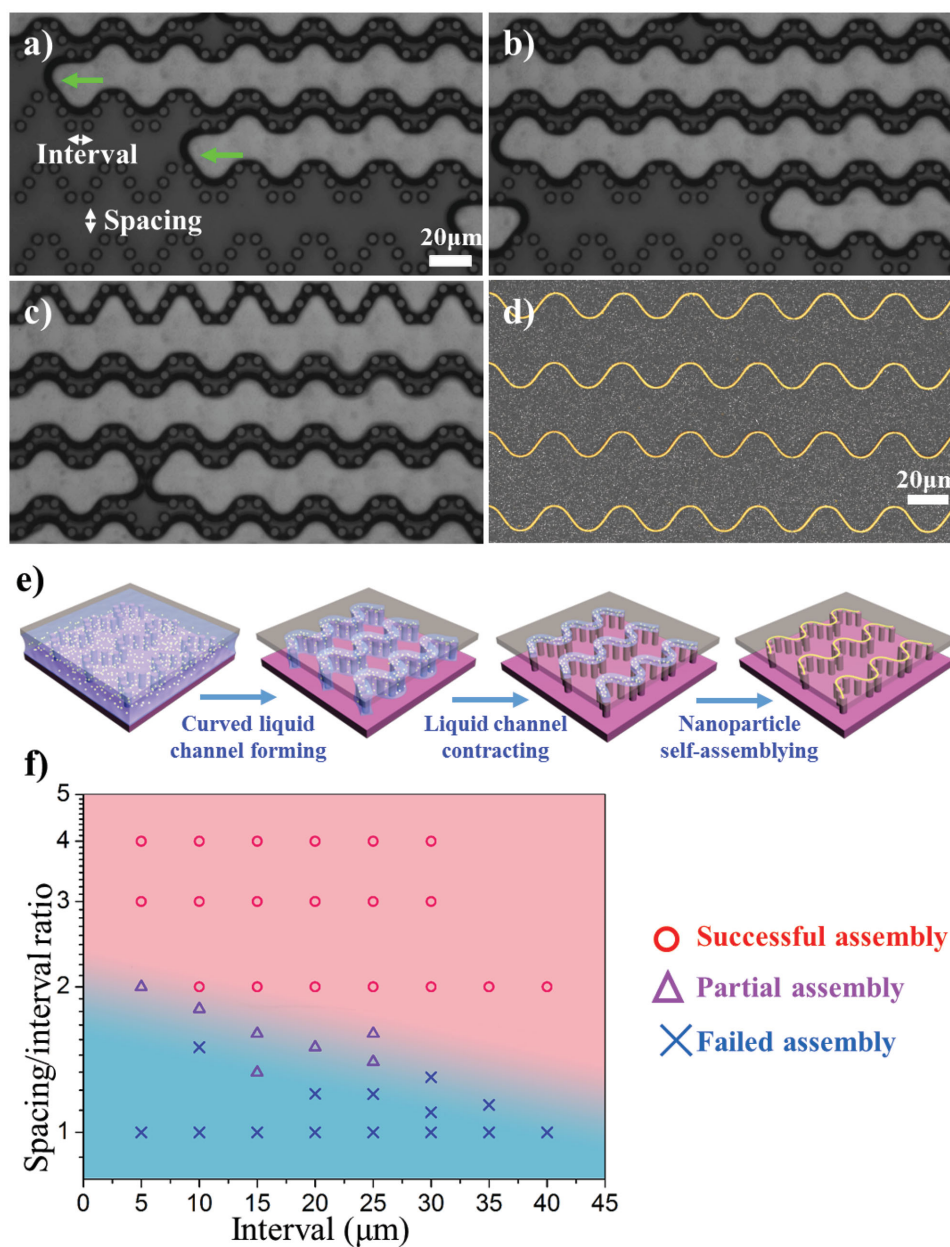


Figure 2. Consecutive liquid bridges lead to precisely designed assembly of NPs. a–c) The transparent glass plate has been chosen as the substrate to observe the formation of liquid bridges. The detailed process was recorded by the dynamic video through optical microscope. Each photograph was taken at three typical stages of the TCL contraction. The green arrows indicate the TCL contracting direction. The white double-headed arrows in the horizontal direction and the vertical direction represent the pillar interval and the spacing, respectively. d) SEM images of AgNPs assembly patterns. e) The schematic illustration of the nanoparticle self-assembly process induced by pillar-patterned template. f) The dependencies map of AgNP assembly on the spacing/interval ratio and the intervals.

of stretchable and sensitive strain sensors attached to selected positions on facial skin, which contain the basic muscle groups for most expression movements. The differential and multielemental muscle movements were monitored with multichannel recorder at real time.

Silver NPs (AgNPs) (Figure S1, Supporting Information) were assembled between the designed pillar-patterned silicon template (Figure S2, Supporting Information) and the flexible substrate (Figure 2a–c). Liquid bridges of certain geometric

configuration, obeying the mathematical consequence of the area-minimizing principle,^[18,19] provide a gradually reduced confined space^[13] for NP aggregation. Finally, close-packed arrays of AgNP nanocurves (Figure S5, Supporting Information) were assembled through this strategy. Also, a single nanoparticle curve can be achieved, as shown in Figure S6 (Supporting Information). Thus, this efficient assembly method is able to align nanomaterials into patterns at nanoscale resolution. Figure 2d presents the AgNPs curves ($R = 0.44$) SEM

image with a false color. After postprocessing of AgNP assembled curves, these structures turned into flexible conductive curves (Figure S7, Supporting Information) down to nanoscopic width and up to centimeter length. The method could be a general strategy to assemble materials into designed patterns. We also achieved conducting polymer (e.g., poly(3-hexyl thiophene), termed as P3HT) curves arrays by using a P3HT toluene solution (Figure S9, Supporting Information).

To get continuous curved liquid bridge arrays for NP assembly, the liquid surface tension and viscosity must be well controlled^[13,26] (Figure S4, Supporting Information). Furthermore, the spacing/interval ratio, as mentioned in Figure 2a, is the key to yielding regularly arranged curve arrays. We invested the dependence of curved nanoparticle assembly arrays on the spacing/interval ratio. Figure 2f gives the dependency map. With the evaporation of the assembly solution, the ordered pillar-patterned template dominates in guiding the rupture of the AgNPs suspension and forming an array of parallel liquid bridges, which is the successful assembly process. The spacing/interval ratio must be large enough to separate the liquid body into many liquid bridges, owing to the minimization of interfacial energies. Actually, the difference between interval and spacing can effectively separate the AgNP solution and guide it into several conductive liquid bridges. In this study, successful patterned AgNP assemblies are formed when the intervals are 20 or 40 μm , and the ratio is 4, respectively. The constantly forming solid–liquid–vapor interface spontaneously contracts along the pillars (Figure S3, Supporting Information). These liquid bridges are same as the shortest path to connect adjacent pillars, meaning the minimum. With arbitrary pillar template designing, we can get more complicated curves by this strategy (Figure S8, Supporting Information).

Through adjusting the pattern of pillar template, arbitrary AgNPs curves with various tortuosity morphologies can be achieved. Figure 3a displays the printed curves with diverse amplitude and period length. The ratio (R) of amplitude (l_1) and period (l_2) is defined to evaluate the tortuosity of various curves. The sensitivity, which is determined by the AgNPs self-assembly curves with different R , has different strain distribution through the curved area. The curves can improve stretchability of these conductive nanoparticle assembly lines on elastomeric substrates. All of these patterns show well conductivity after sintering 2 h at 200 °C. In situ strain-resistance measurements with straight lines, and diverse curve patterns were tested at a strain from 0% to 7% resistive strain sensitivity. The tests were conducted using a custom-built fully automated stretching apparatus with a step resolution of 50 μm . The displacement of the samples was controlled by a linear stage actuated with a micrometer screw driven by a stepper motor. The resistance was measured in real-time using a HIOKI multi-channel recorder at every 20 ms when stretching. The resistance measurements were acquired with accurate synchronization with the displacement. Extensive simulation and in situ testing of serpentine electrodes have shown that such a curved configuration improves maximum stretchability of these patterns on elastomeric substrates, which decrease the sensitivity of resistive response to the strain.^[8,20,21] Figure 3b shows the resistance dependence to the mechanical axial strains $\varepsilon\%$ of AgNPs assembled curves on PDMS elastomeric substrates. With different

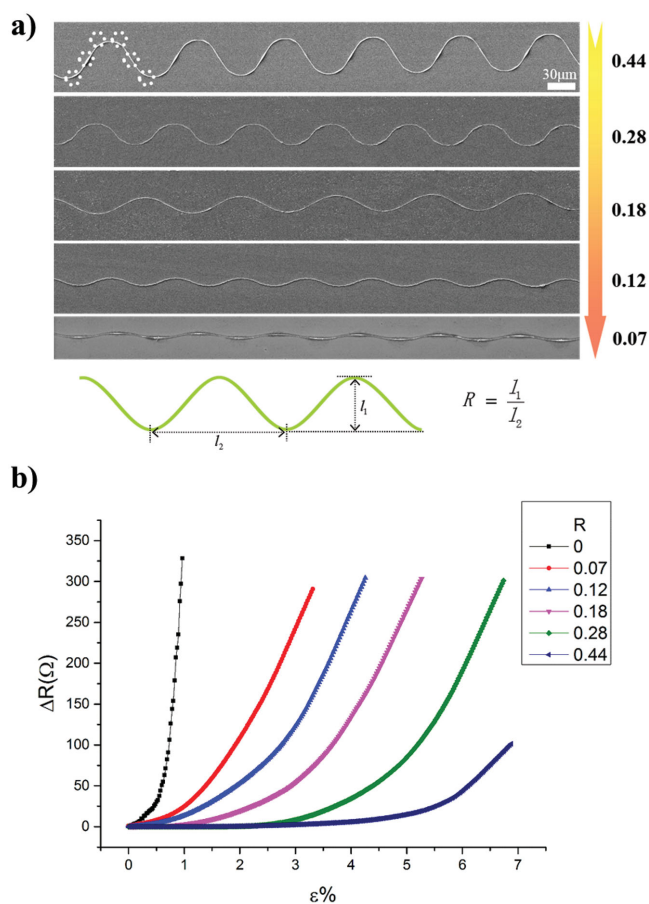


Figure 3. The printed NP curves with diverse curvature or tortuosity and their corresponding stretchable electronics. a) SEM image of the silver nanoparticle curves with different tortuosity morphologies. The ratio (R) of amplitude (l_1) and period (l_2) is defined to evaluate the tortuosity of various curves, which is shown at the right side. b) Electrical resistance of nano-curves with different tortuosity morphologies responded to increasing strain deformation.

amplitude/period ratio (R), the curves performed discriminative resistance responses to the same strain. The main tortuous curve with higher R value has the gentle plot, and the minor tortuous curve with lower R value has the precipitous plot. The theoretical estimation of resistance change for curved electrodes has demonstrated that the strain distribution is not uniform throughout the curved area.^[21b] A high stress and strain concentration was observed in the crest and trough of the curve. The regions with high concentration of strain could cause the separation of nanoparticles, which increased the resistance of NP-based curves. Moreover, increasing the amplitude of the curve could reduce the accumulated strain, which had less effect of the nanoparticles at the crest and trough. Thus, the curves with different R performed discriminative resistance responses to the same strain. Furthermore, it illustrates the advantages of using an optimized meander or curved shape and multiple conductor lines for high deformation of the structures. The sensor with $R = 0.44$ curve had subtle resistance changes from 0% to 3% elastic strains, and started changing critically at 3.4% elastic strain. Rather, the straight line ($R = 0$) had sharp resistance changes and could not bear over 1% strain. The sensor with curves ($R = 0.07$) had a

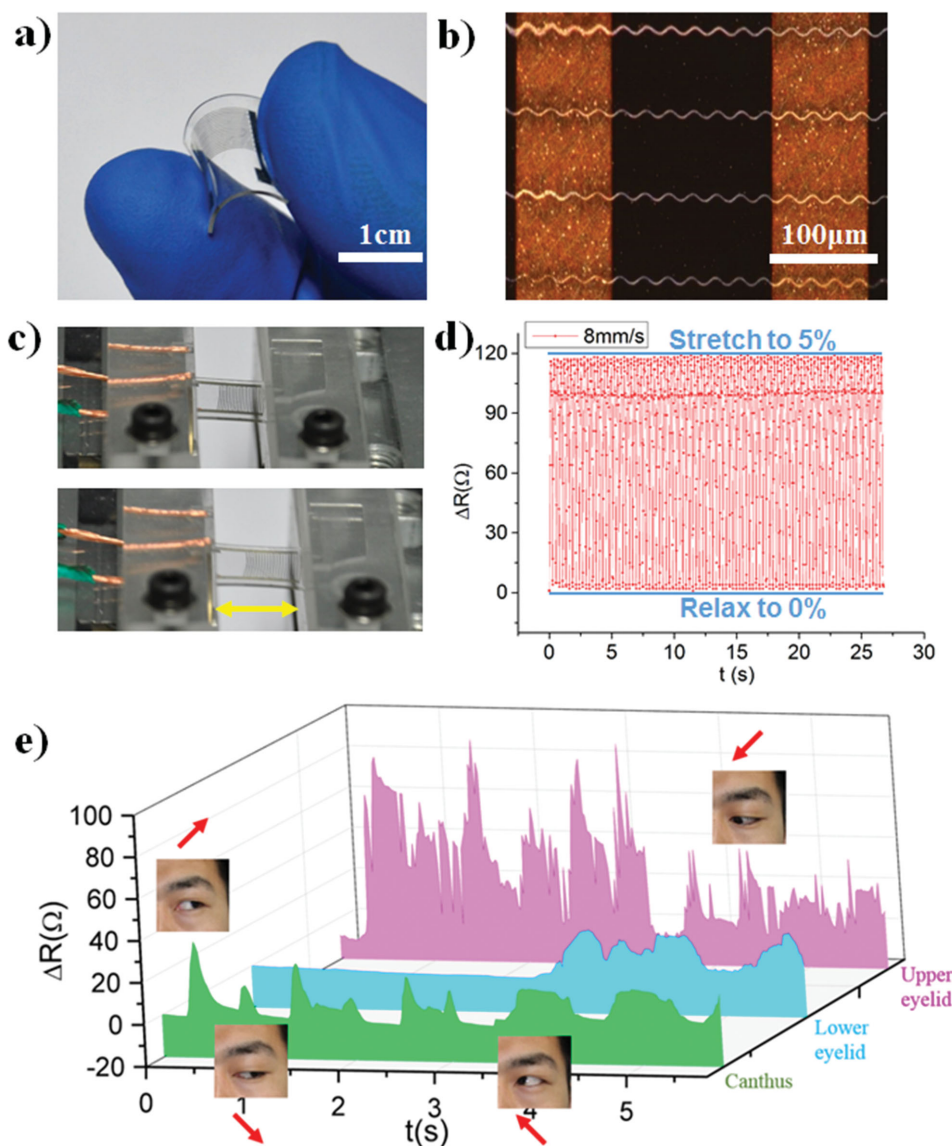


Figure 4. Evaluation of sensing performances. a) Photograph showing sensors coated by designed Au electrode. b) Microscope image of curves between two Au electrodes. c) Photo illustration of the experimental setup, the yellow double-headed arrow showing the stretching direction. d) Electrical resistance responses under different rate of strain change. The durability test under a strain of 5% at a frequency at 4 Hz. e) The real-time monitoring of resistance changes (ΔR) with eyeball movements at four different orientations. The elastomeric sensors were attached at the upper eyelid, lower eyelid, and canthus on facial skin.

slow change from 0% to 3% elastic strains. Sensors with curves ($R = 0.12, 0.18, 0.28$) had different subtle and sharp resistance change stages. With the characteristics of adjustable resistance responses to strain, curves array sensors are the optimal choice for soft or curvilinear surfaces sensing. It also makes resistance responses fitting the multichannel recorder scale.

Based on the discriminative resistance of AgNP assembled curves with different deformation, we adopted AgNP curves arrays (Figure S13, Supporting Information) to integrate on the microelectrode sensor. The continuous AgNP curves were arranged in parallel on comb-like electrodes with 100 μm interval as shown in Figure 4a,b. The PDMS film with 0.8–1.2 mm thickness was used as the substrate for the

curves array sensor. A multichannel electronics data recorder was used to monitor and record the resistance change on the microelectrode sensor (Figure 4c). The AgNP curve flexible sensor processed dynamic mechanical strain between 0% and 5% deformation. After ≈ 1000 cycles, the AgNP curve-based strain sensors still showed a stable and real-time response (Figure 4d). It could be adopted to amplitude and frequency mechanical straining over 4 Hz. The integrated elastomeric sensors were attached on one's face (the upper eyelid, lower eyelid, and canthus) to investigate small strain sensing. As for the detailed real-time monitoring in Figure 4e, when the eyeball rolls in four different orientations, the sensors offer differential resistance responses. By synthesizing these responses, eyeball

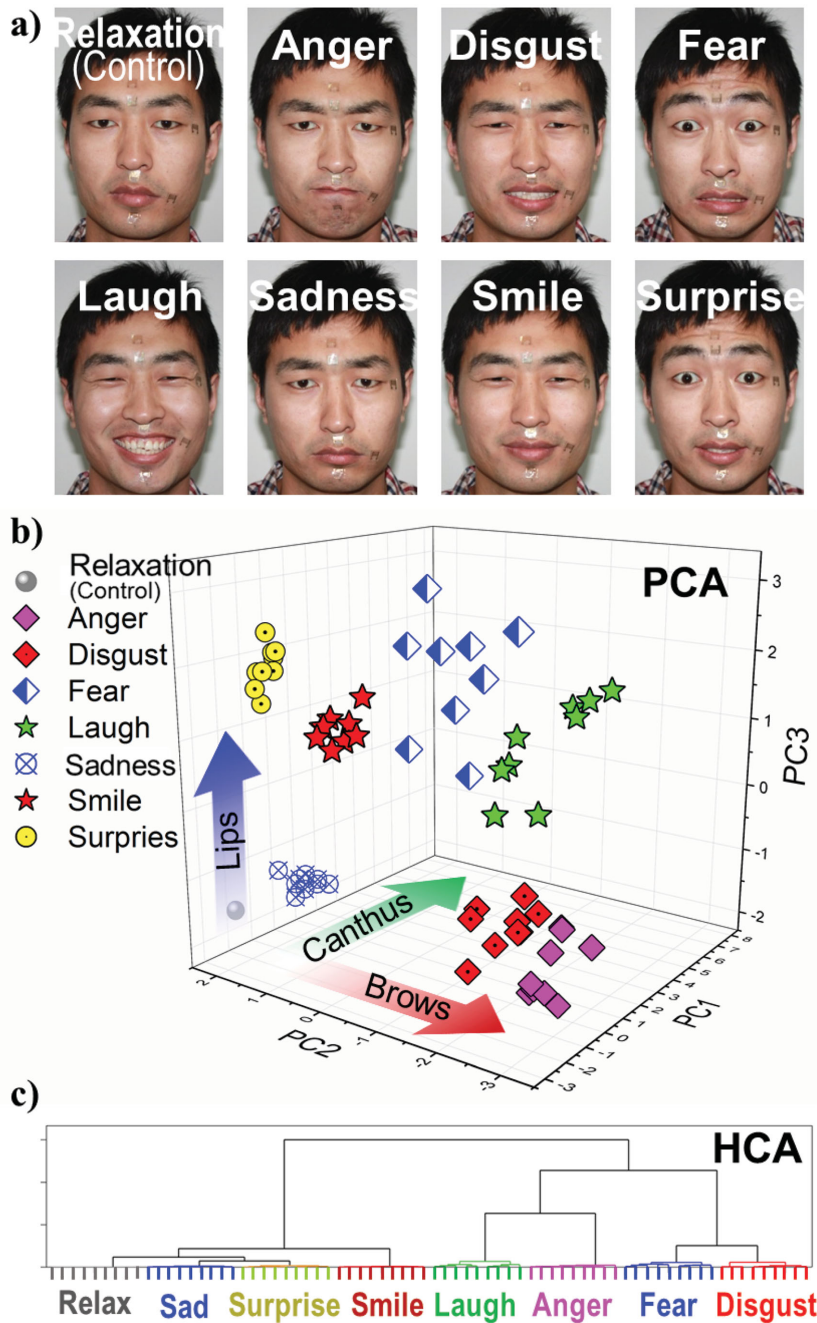


Figure 5. Electronics discriminant analysis of eight facial expression on nanoparticle curves-based strain sensors array and rational analysis. a) The nanocurves array chips were attached at six selective positions on facial skin, which included the characteristic muscle groups. b) 3D representation of PCA result shows a clear clustering of the eight different facial expressions as analytes. c) HCA gives the similarity clustering of the analytes based on the characteristic muscle movement variation trend.

movements can be tracked accurately, which indicates its potential to serve as a wearable micromotion manipulation auxiliary apparatuses for paraplegics.

The sensor can be extended to multichannel monitoring of delicate deformation for human facial expression (Figure S15, Supporting Information). As shown in Figure 5a, six positions were selected on facial skin, which contain the basic muscle

groups^[17] for most expression movements. Eight main facial expressions of emotion (anger, disgust, fear, laughter, sadness, smiling, surprise, and relaxed as control) were investigated. Originating from the distinct resistance changes during facial expression, the principal component analysis (PCA) and hierarchical cluster analysis (HCA) statistical operations were performed.^[22–24] It shows completed and clear classification of all the eight monitored expressions. From the PCA result in Figure 5b, all the expressions are distributed following three directions approximately. The corners of the lips, canthus, and between the brows compose the top three main contributions to the discriminate and cluster analysis (Figure S14 and Tables S1–S7, Supporting Information). Movements between the brows refer to anger, disgust, fear, and sadness, etc., (the most negative expressions). Canthus movements refer to smiling and laughter, (expressions of delight), while movements at the corners of the lips usually promote or enhance certain expressions, like fear, laughter, or surprise. In fact, human facial expressions are generated by several muscle groups. To obtain a happy laughter, all of the muscle groups on the face need to be excited.

The NP curve-based strain sensors can achieve detailed monitoring of the complexed micro muscle group movements.^[25] Actually, the most remarkable application will contribute to skin micromotion manipulation auxiliary apparatuses for paraplegics and quadriplegics. With two or three NP array sensors attached to palpebra, it can perform distinct, detailed, and real-time outputs corresponding to eyeball movement at four orientations. Through delicate movements, a human can operate such an apparatus agilely and with ease. In the near future, with auxiliary devices, manned or unmanned vehicles could be driven by moving eyeballs and lips, which is much less effort than for current operations.

In summary, focused on the tunable flexibility for wearable electronics, we developed a facile fabrication method for electromechanical sensing by assembling AgNP curves via pattern template-induced printing. Through conquering the challenge of droplet three-phase contact line continuous singularity manipulation, the method can realize arbitrary adjustment of tortuosity morphology. The NP curves with various curvatures offer a firm stretching reversibility and tunable sensitivity. The printable NP curves provide the large-scale fabrication for performing sensitive and stable resistance response on deformations, which could run complicated facial expression recognition and contribute the remarkable application on skin micromotion

manipulation auxiliary apparatuses for the paraplegic and quadriplegic people. This print strategy to fabricate flexible electronics and sensors is versatile in application, and will open an efficient avenue for consumer health and electronics products, multifunctionality packaging, and electromechanical sensing in a broad range of medical and biomedical applications.

Experimental Section

Sensor Fabrication and Characterization: A pillar-patterned silicon template with a radius of 5 μm and height of 20 μm was placed horizontally. Then, 10 μL droplet of AgNP/sodium dodecyl sulfate (SDS) hybrid suspension (10–50 mg mL^{-1} AgNPs and 0.5–2 mg mL^{-1} SDS)^[13] was carefully dropped onto the template and covered by a flat PDMS film. Then AgNP curves were printed on the film. Next, AgNP curve arrays were sintered at 200 $^{\circ}\text{C}$ for 2 h. Finally, the Cr/Au interdigitated electrodes (thickness at 5 nm/50 nm) were deposited onto this film using a designed shadow mask (Figure S12, Supporting Information) by a high vacuum thermal evaporation system (PATOR, ATT010), resulting in a highly sensitive and fully integrated strain sensor. The electrical measurement for a single AgNP curve was characterized under ambient conditions, using a Keithley 4200-SCS semiconductor system. The strains were applied by using a home-made stretching equipment. For multianalysis, the multichannel recorder (HIOKI, LR8400) was connected to the sensors.

Data Analysis: The statistical multivariate methods, PCA, linear discriminant analysis (LDA), and hierarchical clustering analysis (HCA),^[22–24] were routinely used to interpret and evaluate the responses from flexible sensor attached on six selected facial positions, providing a graphical output useful to gain an insight into the clustering of the response data, and calculate classification accuracy. Three characteristic values were read out at the peak or nadir of the monitoring resistance curves by the electronics data logger. There were 18 variables for each facial expression to describe the responses on the sensors. The PCA and HCA were carried out using Minitab v16.1.1.0 and the LDA was carried out using SYSTAT v12.02.00.

Supporting Information

Supporting Information is available from the Wiley Online Library or from the author.

Acknowledgements

F. Y. Li and Y. L. Song thank the financial support of 973 Program (No. 2013CB933004), 863 program (No. 2013AA030802), the National Nature Science Foundation (Grant Nos. 51203166, 51473172, 51473173, 21301180, 21303218, and 21203209), and the “Strategic Priority Research Program” of Chinese Academy of Sciences (Grant No. XDA09020000).

Received: September 27, 2015

Revised: November 2, 2015

Published online: December 8, 2015

[1] D. Kim, N. Lu, R. Ma, Y. Kim, R. Kim, S. Wang, J. Wu, S. Won, H. Tao, A. Islam, K. Yu, T. Kim, R. Chowdhury, M. Ying, L. Xu, M. Li, H. Chung, H. Keum, M. McCormick, P. Liu, Y. Zhang, F. Omenetto, Y. Huang, T. Coleman, J. Rogers, *Science* **2011**, *333*, 838.

- [2] a) F. Fan, L. Lin, G. Zhu, W. Wu, R. Zhang, Z. L. Wang, *Nano Lett.* **2012**, *12*, 3109; b) C. Pang, G. Lee, T. Kim, S. M. Kim, H. N. Kim, S. Ahn, K. Suh, *Nat. Mater.* **2012**, *11*, 795.
- [3] J. Park, Y. Lee, J. Hong, Y. Lee, M. Ha, Y. Jung, H. Lim, S. Y. Kim, H. Ko, *ACS Nano* **2014**, *12*, 12020.
- [4] a) D. J. Lipomi, M. Vosgueritchian, B. C. Tee, S. L. Hellstrom, J. A. Lee, C. H. Fox, Z. Bao, *Nat. Nanotechnol.* **2011**, *6*, 788; b) K. Takei, T. Takahashi, J. C. Ho, H. Ko, A. G. Gillies, P. W. Leu, R. S. Fearing, A. Javey, *Nat. Mater.* **2010**, *9*, 821; c) B. C. Tee, C. Wang, R. Allen, Z. Bao, *Nat. Nanotechnol.* **2012**, *7*, 825.
- [5] a) T. Someya, T. Sekitani, S. Iba, Y. Kato, H. Kawaguchi, T. Sakurai, *Proc. Natl. Acad. Sci. USA* **2004**, *101*, 9966; b) T. Someya, Y. Kato, T. Sekitani, S. Iba, Y. Noguchi, Y. Murase, H. Kawaguchi, T. Sakurai, *Proc. Natl. Acad. Sci. USA* **2005**, *102*, 12321; c) S. C. B. Mannsfeld, B. C. Tee, R. M. Stoltenberg, C. V. H. Chen, S. Barman, B. V. O. Muir, A. N. Sokolov, C. Reese, Z. Bao, *Nat. Mater.* **2010**, *9*, 859.
- [6] V. Maheshwari, R. F. Saraf, *Science* **2006**, *312*, 1501.
- [7] J. R. Windmiller, J. Wang, *Electroanalysis* **2013**, *25*, 29.
- [8] J. A. Fan, W. Yeo, Y. Su, Y. Hattori, W. Lee, S. Jung, Y. Zhang, Z. Liu, H. Cheng, L. Falgout, M. Bajema, T. Coleman, D. Gregoire, R. J. Larsen, Y. Huang, J. A. Rogers, *Nat. Commun.* DOI 10.1038/ncomms4266.
- [9] a) R. R. Naik, S. J. Stringer, G. Agarwal, S. E. Jones, M. O. Stone, *Nat. Mater.* **2002**, *1*, 169; b) X. Liu, L. He, J. Zheng, J. Guo, F. Bi, X. Ma, K. Zhao, Y. Liu, R. Song, Z. Tang, *Adv. Mater.* **2015**, *27*, 3273; c) H. Yin, S. Zhao, K. Zhao, A. Muqsit, H. Tang, L. Chang, H. Zhao, Y. Gao, Z. Tang, *Nat. Commun.* DOI: 10.1038/ncomms7430.
- [10] a) T. Kraus, L. Malaquin, H. Schmid, W. Riess, N. D. Spencer, H. Wolf, *Nat. Nanotechnol.* **2007**, *2*, 570; b) W. L. Cheng, N. Y. Park, M. T. Walter, M. R. Hartman, D. Luo, *Nat. Nanotechnol.* **2008**, *3*, 682.
- [11] J. X. Huang, A. R. Tao, S. Connor, R. R. He, P. D. Yang, *Nano Lett.* **2006**, *6*, 524.
- [12] a) W. Han, M. Byun, B. Li, X. C. Pang, Z. Q. Lin, *Angew. Chem. Int. Ed.* **2012**, *51*, 12588; b) J. Xu, J. F. Xia, Z. Q. Lin, *Angew. Chem. Int. Ed.* **2007**, *46*, 1860; c) B. Qin, H. Chen, H. Liang, L. Fu, X. Liu, X. Qiu, S. Liu, R. Song, Z. Tang, *J. Am. Chem. Soc.* **2010**, *132*, 2886.
- [13] B. Su, C. Zhang, S. Chen, X. Zhang, L. Chen, Y. Wu, Y. Nie, X. Kan, Y. Song, L. Jiang, *Adv. Mater.* **2014**, *26*, 2501.
- [14] S. Chen, M. Su, C. Zhang, M. Gao, B. Bao, Q. Yang, B. Su, Y. Song, *Adv. Mater.* **2015**, *27*, 3928.
- [15] J. N. Bassili, *J. Pers. Soc. Psychol.* **1979**, *37*, 2049.
- [16] K. H. Kim, S. W. Bang, S. R. Kim, *Med. Biol. Eng. Comput.* **2004**, *42*, 419.
- [17] B. M. Waller, A. M. Burrows, J. J. Cray, *Emotion* **2008**, *8*, 435.
- [18] C. Isenberg, *The Science of Soap Films and Soap Bubbles*, Tieto Ltd., Clevedon, England **1978**, p. 53.
- [19] F. J. Almgren, J. E. Taylor, *Sci. Am.* **1976**, *235*, 82.
- [20] H. Sagan, *Space-Filling Curves*, Springer Science & Business Media, Heidelberg, Germany, **2012**.
- [21] a) P. Gutruf, S. Walia, M. N. Ali, S. Sriram, M. Bhaskaran, *Appl. Phys. Lett.* **2014**, *104*, 021908; b) M. Gonzalez, F. Axisa, M. V. Bulcke, D. Brosteaux, B. Vandeveld, J. Vanfleteren, *Microelectron. Reliab.* **2008**, *48*, 825.
- [22] J. J. Lavigne, E. V. Anslyn, *Angew. Chem. Int. Ed.* **2001**, *40*, 3119.
- [23] P. Anzenbacher, F. Y. Li, A. M. Palacios, *Angew. Chem. Int. Ed.* **2012**, *51*, 2345.
- [24] Y. Huang, F. Y. Li, M. Qin, L. Jiang, Y. L. Song, *Angew. Chem. Int. Ed.* **2013**, *125*, 7437.
- [25] E. Roh, B. Hwang, D. Kim, B. Kim, N. Lee, *ACS Nano* **2015**, *9*, 6252.
- [26] K. Kuroishi, M. Chen, Y. Kitamoto, T. Seki, *Electrochim. Acta* **2005**, *51*, 867.